

NUMERICAL ANALYSIS OF THE AERODYNAMICS OF THE AURORA AIRCRAFT BY AN INVISCID/VISCOUS INTERACTION METHOD

J. Su

Aerodynamic Laboratory, Institute for Aerospace Research,
National Research Council of Canada, Ottawa, Canada

J.T. Conway

Agder College, Grimstad, Norway

Abstract

The PMAL3D computer code has been extended to an aircraft configuration with propellers by embedding a nonlinear actuator disk theory developed by Conway in the PMAL3D inviscid/viscous interaction code developed at AL/IAR/NRC. The actuator disk model was coupled to PMAL3D by introducing the time-averaged velocity field induced by each propeller actuator disk as a modification of the free stream. The theory of the panel method, integral boundary layer method, and the actuator disk model are briefly presented in the present paper. This study has included both propeller and viscous effects on the aerodynamics of an aircraft and presented detailed numerical analyses and discussions of the aerodynamics for the Aurora configuration.

1 Introduction

The numerical analysis of three-dimensional viscous compressible flows is becoming increasingly important for the aerodynamic design of modern aircraft. The viscous/inviscid interaction methods are much more attractive than the advanced Navier-Stokes solvers for these problems since they can yield, at a much lower cost, results that match experimental data well. For low speed subsonic flows as considered here, a panel method is sufficiently accurate for the outer inviscid flow. The inner viscous boundary layer flow can be solved using either a finite difference method or an integral method. Cebeci et al. [1], Mclean [2] and

Matsuno [3] among many others developed finite difference methods for computing the three-dimensional turbulent boundary layer development on wings. All these approaches must introduce a turbulence model to solve the turbulent boundary layer equations. The method used by this paper, i.e., an integral method, achieves a considerable simplification of the problem with little loss in accuracy by solving the three dimensional integral rather than differential boundary layer equations. The details of the boundary layer velocity profiles resulting from the finite difference methods can be useful for some problems. However, for the application considered here, the efficiency of the integral approach more than compensates for any loss of accuracy in the velocity profile prediction, as the integral properties of the boundary layer such as the momentum thickness are not very sensitive to the velocity profile assumptions.

The interaction of the propellers with the Aurora configuration was calculated by embedding the nonlinear actuator disk theory [6,7,8] in the PMAL3D inviscid/viscous interaction code developed at AL/IAR/NRC. The potential solver of PMAL3D calculates the Neumann potential flow external to an aerodynamic configuration, with the normal velocities everywhere on the surfaces of the configuration specified by the user. Wake surfaces have zero normal velocities and are positioned approximately parallel to the local flow. The actuator disk theory has previously been applied to the inviscid flow problem for the Aurora configuration [9]. This study has

considered viscous effects and presented more detailed numerical analyses and discussions of the aerodynamics for the Aurora configuration.

2 Numerical Method

The numerical method is based on interactive boundary layer theory, and involves interaction between inviscid potential and boundary layer solutions. The potential solution is obtained using a panel method and the boundary layer solution is obtained from the three dimensional integral boundary layer equations. The actuator disk model developed by Conway [6,7,8] was coupled to the potential solution by introducing the time-averaged velocity field induced by each propeller actuator disk as a modification of the free stream. The theory of the panel method, integral boundary layer method, and the actuator disk model are briefly given below.

2.1 PMAL3D potential panel method

For an incompressible potential flow, the disturbance potential φ satisfies Laplace's differential equation

$$\nabla^2 \varphi = 0 \quad (1)$$

By applying Green's theorem to the above equation, we obtain the integral equation which the PMAL3D panel method is based on

$$\begin{aligned} \varphi(p) = & \frac{1}{4\pi} \int_{S_b} \varphi \frac{\partial}{\partial n} \left(\frac{1}{r} \right) ds - \frac{1}{4\pi} \int_{S_b} \frac{1}{r} \frac{\partial \varphi}{\partial n} ds \\ & + \frac{1}{4\pi} \int_{S_w} \Delta \varphi \frac{\partial}{\partial n} \left(\frac{1}{r} \right) ds \end{aligned} \quad (2)$$

where S_b is the body surface, S_w is the wake surface and n denotes the normal direction to the body surface. $\Delta(\cdot)$ indicates the difference between the upper and lower wake surfaces.

The numerical procedure of solving the above integral equation by the panel method involves several steps. The first step is to define the surface geometry of the configuration and approximate the surface by a number of panels. A matrix of influence coefficients is then formed. This represents a set of simultaneous linear algebraic equations resulting from a

discretization of the above integral equation. The solution to these equations provides the surface doublet distribution from which the surface velocities, pressures and body forces/moments can be obtained. In PMAL3D, the surface geometry is approximated by quadrilateral panels and in each panel constant source and doublet distributions are assumed, resulting in the so-called low-order panel method.

Equation (2) becomes after discretization

$$\begin{aligned} & \sum_{k=1}^{N_B} (C_{jk} \varphi_k) + \sum_{m=1}^{N_W} (C_{jm} \Delta \varphi_{w_m}) \\ & = \sum_{k=1}^{N_B} B_{jk} \left(\frac{\partial \varphi}{\partial n} \right)_k \quad j=1, \dots, N_B \end{aligned} \quad (3)$$

where N_B and N_W are the number of body surface and wake panels respectively. The quantities B_{jk} and C_{jk} are the influence coefficients for the constant source and doublet distributions respectively on panel k acting on the control point on panel j .

Equation (3) is further manipulated to eliminate the wake strengths as unknown by taking into account the relationship between the wake strength at the separation line and the potential values on the body shedding panels. The result is a matrix equation with the body surface potential as the unknown and a calculated right-hand side that is a function of the body normal velocities

$$[LHS]\{\varphi\} = \{RHS\} \quad (4)$$

which can be solved by a standard program.

The actuator disk model was coupled to PMAL3D by introducing the velocity field induced by each propeller actuator disk as a modification of the free stream. Defining V_A to be the velocity field induced by all the propeller actuator disks, The strength σ of the surface source distribution is determined by

$$\sigma = -(\mathbf{V}_\infty + \mathbf{V}_A) \cdot \mathbf{n} \quad (5)$$

This coupling procedure makes the simplifying assumptions that both the disk loading and the slipstreams remain axisymmetric. The velocity field V_C consisting of the free stream and the velocity induced by the singularities on the

surface of the configuration satisfies equation (1) and hence

$$\nabla^2 V_C = 0 \quad (6)$$

The velocity V_A induced by the actuator disks satisfies the Poisson equation

$$\nabla^2 V_A = -\Omega \quad (7)$$

where Ω is the vorticity determined by the axisymmetric slipstream solutions. Hence the combined solution consisting of $V = V_C + V_A$ satisfies both equation (7) and the Neumann no penetration boundary condition

$$\mathbf{V} \cdot \mathbf{n} = 0 \quad (8)$$

2.2 Boundary layer integral method

Integral prediction methods for three dimensional turbulent boundary layers are most readily described in a streamline coordinate system (s, n) on the body surface with s being in the streamwise direction and n being in the normal direction to the streamline. The integral equations in this coordinate system are:

s momentum integral equation

$$\begin{aligned} \frac{\partial \theta_{11}}{\partial s} + \frac{\partial \theta_{12}}{\partial n} + \frac{\theta_{11}}{U} \frac{\partial U}{\partial s} (2 + H) \\ + \frac{\partial \gamma}{\partial n} (\theta_{11} - \theta_{22}) = \frac{C_f}{2} \end{aligned} \quad (9)$$

n momentum integral equation

$$\begin{aligned} \frac{\partial \theta_{21}}{\partial s} + \frac{\partial \theta_{22}}{\partial n} + \frac{2}{U} \frac{\partial U}{\partial s} \theta_{21} + \frac{\theta_{11}}{U} \frac{\partial U}{\partial n} (1 + H + \frac{\theta_{22}}{\theta_{11}}) \\ + 2 \frac{\partial \gamma}{\partial n} \theta_{21} = \frac{C_f}{2} \tan \beta \end{aligned} \quad (10)$$

entrainment equation

$$\begin{aligned} \frac{\partial(\delta - \delta_1^*)}{\partial s} - \frac{\partial \delta_2^*}{\partial n} \\ = F(H_{\delta - \delta_1^*}) - (\delta - \delta_1^*) \left[\frac{\partial U}{U \partial s} + \frac{\partial \gamma}{\partial n} (1 - e) \right] \end{aligned} \quad (11)$$

where entrainment constant $e=0.5$ in diverging flow ($\partial \gamma / \partial n > 0$) and $e=0.1$ in converging flow ($\partial \gamma / \partial n < 0$); $F(H_{\delta - \delta_1^*})$ is Head's entrainment function; U is the resultant velocity at boundary layer edge; shape factor $H = \delta_1^* / \theta_{11}$; shape

factor $H = (\delta - \delta_1^*) / \theta_{11}$; C_f is the skin friction coefficient; δ is the boundary layer thickness; β is the angle between an external streamline and the corresponding limiting streamline; γ is the streamline direction with respect to x . The displacement and momentum thicknesses are given by

$$\begin{aligned} \delta_1^* &= \int_0^\delta \left(1 - \frac{u}{U}\right) d\zeta, & \delta_2^* &= -\int_0^\delta \frac{v}{U} d\zeta \\ \theta_{11} &= \int_0^\delta \frac{u}{U} \left(1 - \frac{u}{U}\right) d\zeta, & \theta_{12} &= \int_0^\delta \frac{v}{U} \left(1 - \frac{u}{U}\right) d\zeta \\ \theta_{21} &= -\int_0^\delta \frac{uv}{U^2} d\zeta, & \theta_{22} &= -\int_0^\delta \frac{v^2}{U^2} d\zeta \end{aligned}$$

where u is the streamwise boundary layer velocity component; v is the crossflow boundary layer velocity component; ζ is the coordinate in the normal direction to surface. Mager's form for the crossflow

$$\frac{v}{u} = \left(1 - \frac{\zeta}{\delta}\right)^2 \tan \beta \quad (12)$$

and Cumsty and Head's form for the streamwise velocity profile,

$$\frac{u}{U} = \left(\frac{\zeta}{\delta}\right)^{\frac{H-1}{2}} \quad (13)$$

are used here. Equations (12) and (13) enable the crossflow integral thicknesses to be simply expressed as functions of H , θ_{11} and $\tan \beta$.

The details of the numerical integration of the above integral equation set is given in [4,5].

2.3 Nonlinear actuator disk model

An actuator disk models the time-averaged slipstream of a propeller, which is a vortical flow region obeying the Poisson equation with the vorticity as the source term. If the vorticity is known, the swirl velocity can be easily constructed for such an axisymmetric system using Stokes's theorem. The axial and radial components of velocity are induced by the azimuthal component of the vorticity, which is equivalent to an axisymmetric distribution of ring vortices. The nonlinear actuator disk theory

calculates these velocity components by discretizing the slipstream azimuthal vorticity axially into vortex disks. For essentially arbitrary radial variation of vorticity within such a disk, the velocities induced by the disk can be stated in terms of complete elliptic integrals and elementary functions. The velocities induced by the distribution of vortex disks representing the slipstream vorticity can then be obtained in closed form for a lightly loaded propeller [6] by analytical integration in the axial direction, or by numerical axial integration for a heavily loaded propeller [7,8].

3 Results and Discussions

The panel model used for the Aurora calculations is shown in figure 1. In total, 1792 panels with 608 panels for the wings are used for calculating the numerical results presented in this paper.

Figure 2 shows the pressure distributions (potential solution) for the Aurora without propellers at an incidence $\alpha=6^\circ$.

The pressure distributions with four propellers rotating in the same direction (mode A) is shown in figure 3 with a thrust coefficient $CT = T / (\rho_\infty n^2 D^4) = 0.349$ (which is equivalent to a thrust coefficient based on disk area of $CTh = T / (1/2 \rho_\infty V_\infty^2 S) = 2.93$) and an advance ratio $J=0.552$ (Case 1). Here T is the propeller thrust, ρ_∞, V_∞ are the upstream density and speed, n is the revolutions per second, D is the propeller diameter, and S is the propeller disk area. The upstream speed is $V_\infty=38.61$ m/sec and angle of attack is $\alpha=6^\circ$. With this low aircraft speed and quite high thrust coefficient CTh , it is noticed from figure 3 that the propellers have substantial effects on the aerodynamics of the aircraft, especially the wings and tails. From figure 13 which gives the aerodynamics force and moment coefficients for this case, it is observed that the lift coefficient increased by 132% over that without propellers. The other force and moment coefficients also change significantly. It is further noticed that the rolling and yaw moment coefficients are of the same magnitude as the pitching moment

coefficients due to the asymmetric aerodynamics of the four propellers. Similar results are presented in figures 4, 5 and 13 for four propellers assumed rotating in a symmetric state (mode B) and three propellers rotating in the same direction.

A quite interesting comparison between modes A and B is given in figure 6 which shows the pressure difference on the configuration (B-A). It is observed that the difference is significant at the righthand wing and tail which is quite predictable since the propellers rotate in opposite directions for modes A and B, while the difference at the lefthand wing and tail is very small even in this high thrust coefficient (in terms of CTh). The same conclusion can be drawn for the comparison of mode A with the three-propeller case as shown in figure 7. Pressure differences between modes A, B and the three-propeller case are given in figures 8 and 9 with a thrust coefficient $CT=0.234$ (which is equivalent to $CTh=0.17$) and an advance ratio $J=1.876$ (Case 2), and in figures 10 and 11 with a thrust coefficient $CT=0.226$ (which is equivalent to $CTh=0.10$) and an advance ratio $J=2.392$ (Case 3). The same conclusion as the above high thrust coefficient is drawn for these two cases but in smaller magnitudes of differences. Figure 12 presents the pressure difference between the four propeller (mode A) and no propeller cases.

Figure 14 shows the aerodynamics force and moment coefficients for a thrust coefficient $CT=0.234$, an advance ratio $J=1.876$, upstream speed $V_\infty=131.27$ m/sec, and kinematic viscosity $\nu=3.53 \times 10^{-5}$ m²/sec. Figure 15 shows the aerodynamics force and moment coefficients for a thrust coefficient $CT=0.226$, an advance ratio $J=2.392$, upstream speed $V_\infty=167.31$ m/sec, and kinematic viscosity $\nu=7.91 \times 10^{-4}$ m²/sec. For these cases the aerodynamics effects of the propellers are visible but not substantial. The rolling and yaw moments in these two cases are much less than the pitching moment, which means the asymmetric effect of the propellers is quite small.

From the above discussion it is also concluded that for the Aurora configuration

using a half model for measuring lift, drag and pitching moment may be physically sound for practical conditions. At last, a comparison of the present results with data from [10] is shown in figure 16. Although the advance ratio and other physical conditions are unknown for the data from [10], which makes this comparison not very rigorous, it is still very encouraging that the present results match very well with those data for the case of the thrust coefficient $CT_h=0.1$.

Finally, we noticed that while no convergent viscous result is obtained for Case 1 which has high thrust coefficient and low aircraft speed, generally five iterations are required to reach convergent viscous results for Cases 2 and 3. From our calculations, we also found that the viscous effects on the Aurora aerodynamics are quite small at an incidence $\alpha \leq 8^\circ$ for Cases 2 and 3 where no separation occurred.

4 Conclusions

The PMAL3D computer code has been extended to an aircraft configuration with propellers by embedding the nonlinear actuator disk theory developed by Conway [6,7,8] in the PMAL3D inviscid/viscous interaction code developed at AL/IAR/NRC. Numerical analyses have been carried out for three cases with the Aurora configuration by using the code. At the low aircraft speed and high thrust coefficient CT_h (like in a takeoff situation, case 1), the propellers may have substantial effects on the aerodynamics of the aircraft, especially the wings and tails. The total force and moment coefficients may change significantly. It is also to be noted that the rolling and yaw moment coefficients are of the same magnitude as the pitching moment coefficients due to the asymmetric aerodynamics of the four propeller case in the condition of low aircraft speed and high thrust coefficient CT_h . In the cruise conditions (e.g. cases 2 and 3), the aerodynamic effects of the propellers are visible but not substantial. The rolling and yaw moments in this situation are much less than the pitching moment, which means the asymmetric effect of the propellers is quite small. It is also concluded

that for the Aurora configuration using a half model for measuring lift, drag and pitching moment may be physically sound for practical conditions.

Acknowledgements

This study was made possible by the support of the Department of National Defence of Canada. The authors would like to acknowledge many helpful discussions with Dr. Norman Ball of the National Research Council of Canada.

References

- [1] Cebeci T, Kaups K and Ramsey J A. A general method for calculating three-dimensional compressible laminar and turbulent boundary layers on arbitrary wings. *NASA CR-2777*, Jan. 1977.
- [2] McLean J D. Three-dimensional turbulent boundary layer calculations for swept wings. *AIAA Paper 77-3*, Jan. 1977.
- [3] Matsuno K. A vector-oriented finite difference scheme for calculating three-dimensional compressible laminar and turbulent boundary layers on practical wing configurations. *AIAA Paper 81-1020*, June 1981.
- [4] Crabbe R S. A simple numerical method to compute viscous lift loss of wings. *Journal of Aircraft*, Vol. 35, No. 1, pp 27-32, 1998.
- [5] Su J and Crabbe R S. Numerical prediction of aerodynamic performance of a complete aircraft with contaminated wings and flaps. *Proceedings of 1998 ASME Fluids Engineering Division Summer Meeting*, Washington DC, FEDSM98-4984, June 1998.
- [6] Conway J T. Analytical solutions for the actuator disk with variable radial distribution of load. *Journal of Fluid Mechanics*, Vol. 297, August 1995.
- [7] Conway J T. Exact actuator disk solutions for non-uniform heavy loading and slipstream contraction. *Journal of Fluid Mechanics*, Vol. 365, June 1998.
- [8] Conway J T. Prediction of the performance of heavily loaded propellers with slipstream contraction. *Journal of the Canadian Aeronautics and Space Institute*, Vol. 44, No. 3, September 1998.
- [9] Conway J T and Su J. PMAL propeller-induced asymmetric flow calculations for the Aurora aircraft using embedded nonlinear actuator disks. *The 46th Annual Conference of the Canadian Aeronautics and Space Institute*, May 2-5, 1999.
- [10] Meyer J E, Torrillo J E and Feistel T W. Aerodynamic Data for Loads Analysis. *Lockheed Aircraft Corporation Report 13134*, 1958.

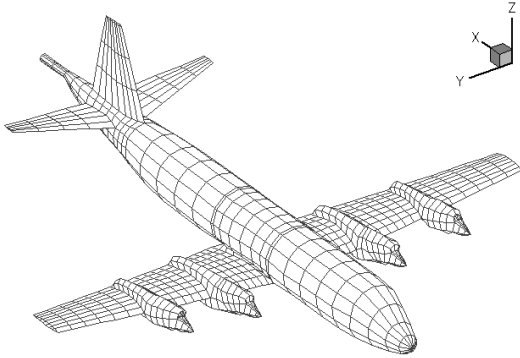


Figure 1 Paneling for the Aurora configuration

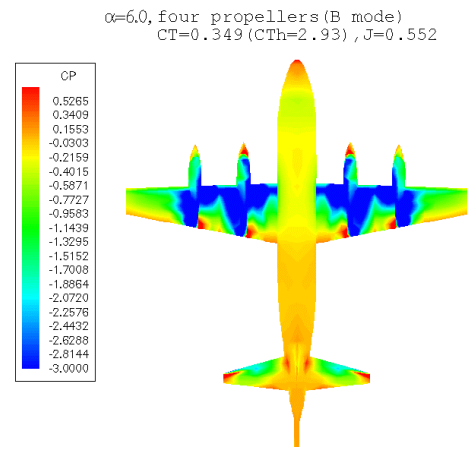


Figure 4 Pressure contour for the Aurora with four propellers rotating in a symmetric state (mode B)

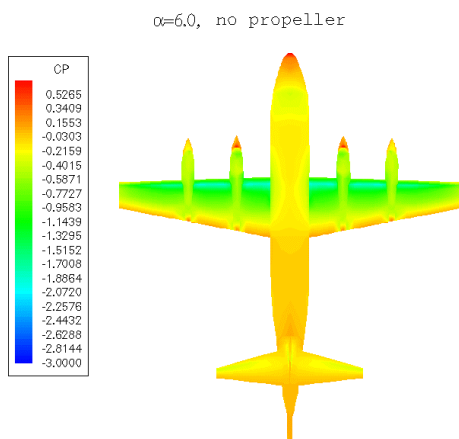


Figure 2 Pressure contour for the Aurora without propellers

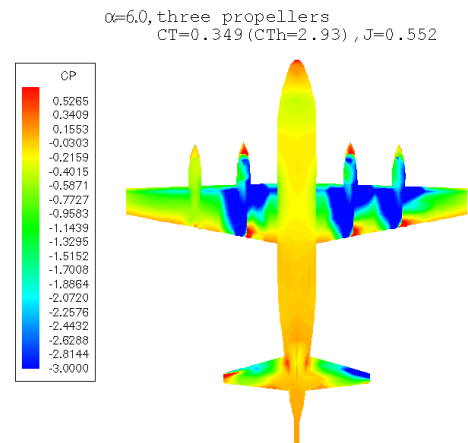


Figure 5 Pressure contour for the Aurora with three propellers rotating in the same direction

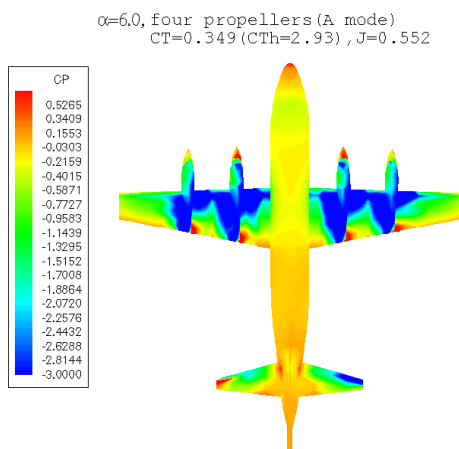


Figure 3 Pressure contour for the Aurora with four propellers rotating in the same direction (mode A)

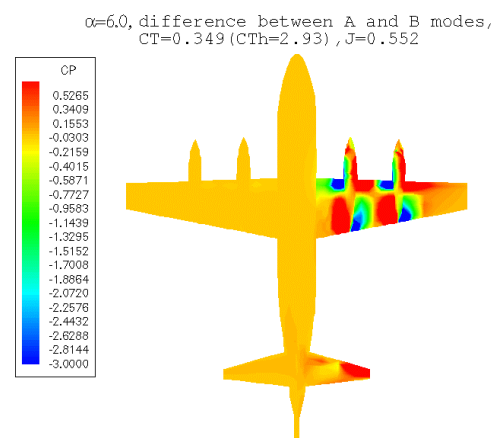


Figure 6 Pressure difference between modes A and B

NUMERICAL ANALYSIS OF THE AERODYNAMICS OF THE AURORA AIRCRAFT BY AN INVISCID/VISCOUS INTERACTION METHOD

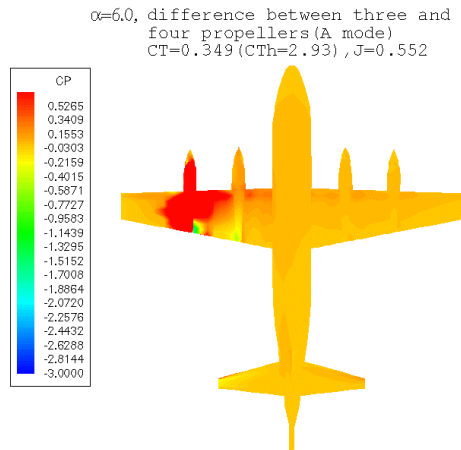


Figure 7 Pressure difference between three propellers and mode A

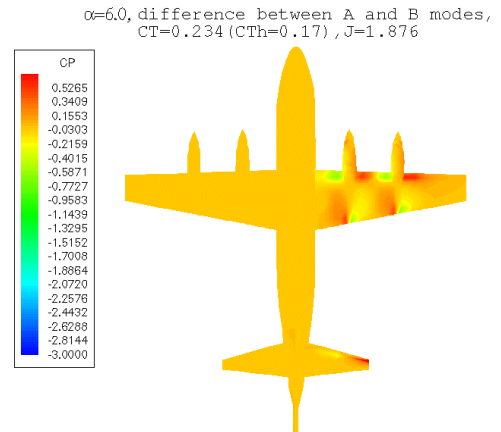


Figure 10 Pressure difference between modes A and B

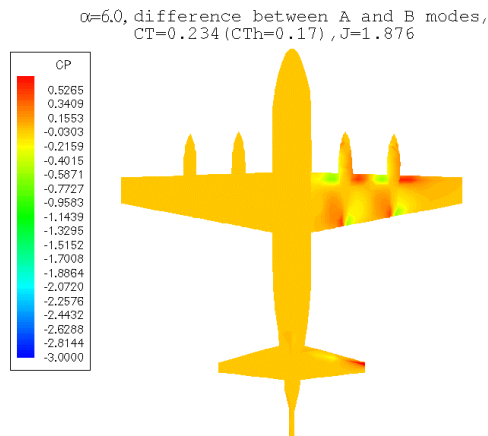


Figure 8 Pressure difference between modes A and B

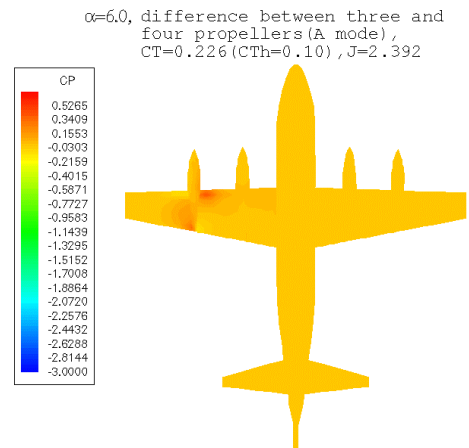


Figure 11 Pressure difference between three propellers and mode A

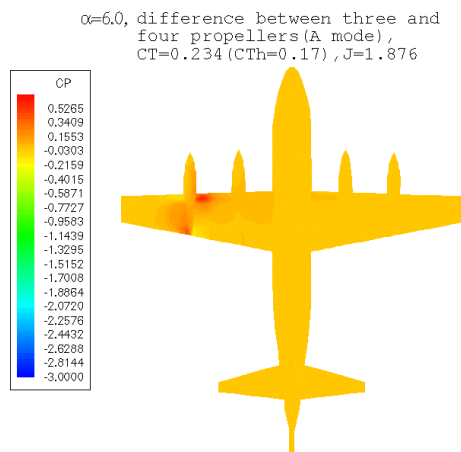


Figure 9 Pressure difference between three propellers and mode A

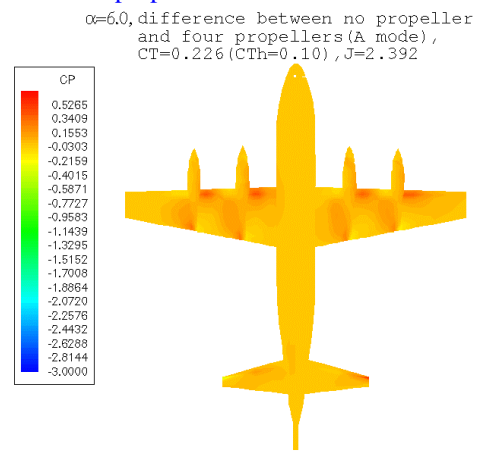


Figure 12 Pressure difference between with four propellers (mode A) and without propeller

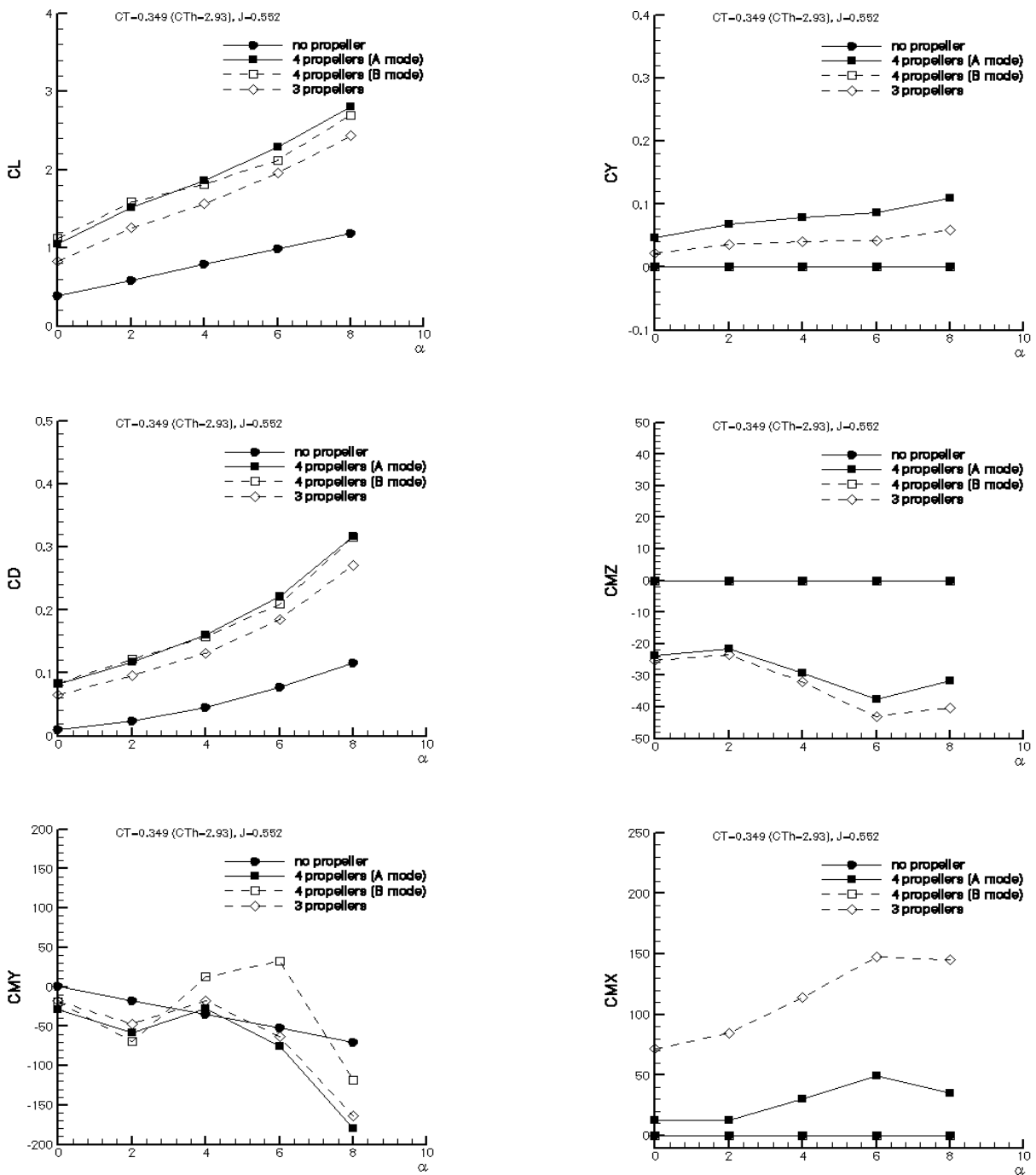


Figure 13 Comparisons of the aerodynamics coefficients for the Aurora, $CT=0.349(CTh=2.93)$, $J=0.552$

NUMERICAL ANALYSIS OF THE AERODYNAMICS OF THE AURORA AIRCRAFT BY AN INVISCID/VISCOUS INTERACTION METHOD

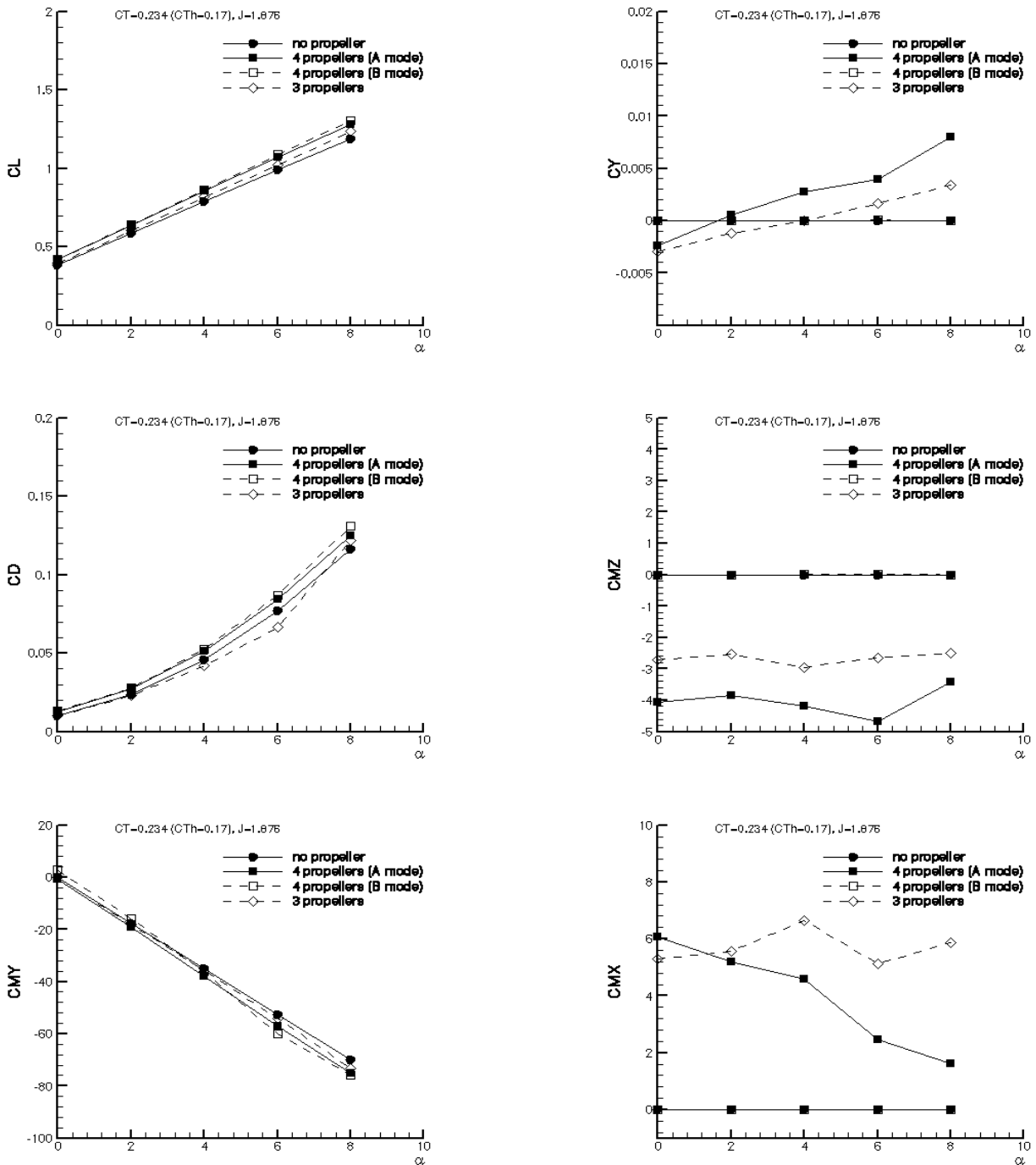


Figure 14 Comparisons of the aerodynamics coefficients for the Aurora, $CT=0.234$ ($CTh=0.17$), $J=1.876$

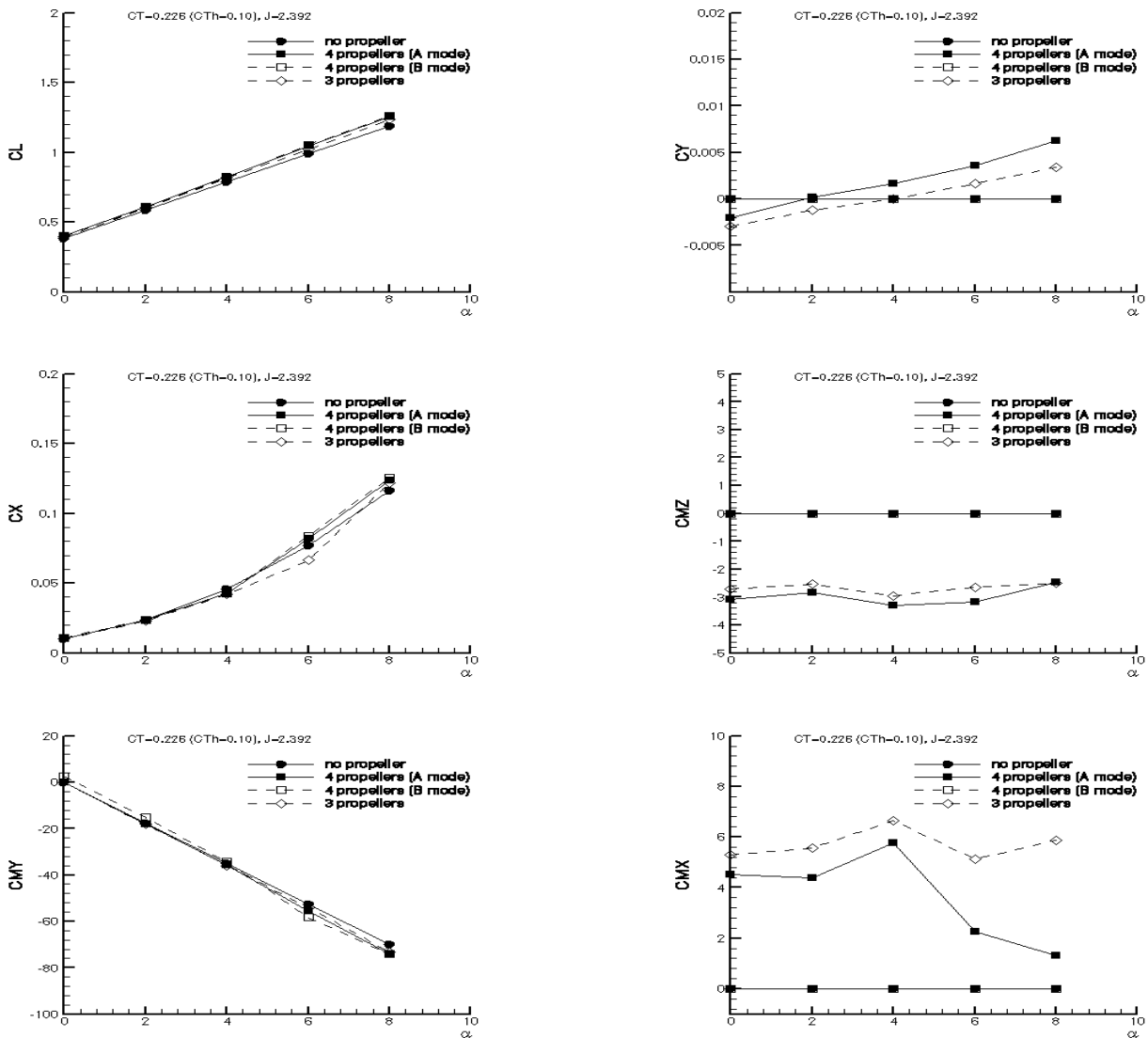


Figure 15 Comparisons of the aerodynamics coefficients for the Aurora, $CT=0.226(CTh=0.10)$, $J=2.392$

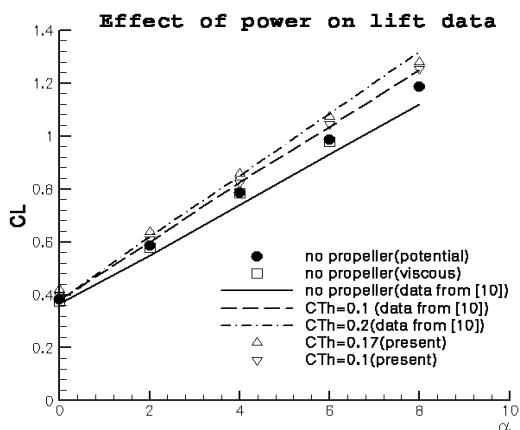


Figure 16 Comparison of the present results with the data from [10]